Analytical and Bioanalytical Chemistry (2022) 414:4217–4225
https://doi.org/10.1007/s00216-022-04074-8

RESEARCH PAPER

Colorimetric sensing strategy for detection of cysteine, phenol cysteine, and phenol based on synergistic doping of multiple heteroatoms into sponge-like Fe/NPC nanozymes

Yuting Xue[1] · Haotian Zhong[1] · Bin Liu[1] · Ruixue Zhao[1] · Jun Ma[1] · Zhengbo Chen[1] · Kai Li[1] · Xia Zuo[1]

Received: 3 March 2022 / Revised: 2 April 2022 / Accepted: 6 April 2022 / Published online: 25 April 2022

Abstract

Nanozymes have both the high catalytic activity of natural enzymes and the stability and economy of mimetic enzymes. Research on nanozymes is rapidly emerging, and the continuous development of highly catalytic active nanozymes is of far-reaching significance. This work reports heteroatomic nitrogen (N) and phosphorus (P) double-doped mesoporous carbon structures and metallic Fe coordination generated sponge-like nanozymes (Fe/NPCs) with good peroxidase activity. On this basis, we constructed a highly sensitive colorimetric sensor with cysteine and phenol as simulated analytes using Fe/NPCs nanozymes, and the response limits reached 53.6 nM and 5.4 nM, respectively. Besides, the method has high accuracy in the detection of cysteine and phenol at low concentrations in serum and tap water, which lays a foundation for application in the fields of environmental protection and biosensors.

Keywords Nanozymes · Heteroatom doping · Colorimetric · Cysteine · Phenol

Introduction

Natural enzymes have attracted wide attention due to their amazing catalytic efficiency and substrate specificity. Due to their poor stability and high cost, the activity and biochemical application of enzymes in complex environments are limited [1, 2]. To solve this problem, researchers are committed to developing new and more effective artificial nanozymes. Nanozymes are a series of nanomaterials with enzyme mimicking characteristics, which have the advantages of low preparation cost, high stability, diverse functions, and modifiable properties [3–5].

Accordingly, various functional nanomaterials, such as precious metals, metal oxides, organic metal frameworks, and carbon nanozymes, have been proved to have HRP-like activities [6–8]. Metal nanozymes have good catalytic activity, and how to increase the number of active centers and reactive oxygen species of carbon nanozymes is a challenge. Studies have shown that heteroatom nitrogen (N) doping into carbon skeleton enhances peroxidase activity [9–14]. Moreover, the introduction of diversified heteroatoms, such as B, P, or S, can also greatly improve the catalytic efficiency of carbon nanomaterials [15–18]. Currently, diverse heteroatom-doped nanozymes are not common. Therefore, heteroatom doping might be an effective strategy to improve the performance of carbon nanozymes (Scheme 1).

Phenolic compounds represented by phenol are widely present in industrial wastewater, feces, and nitrogen-containing organic substances, and are used in various modern industries, including food, pharmaceuticals, oil refining, and coatings [19–25]. However, phenolic compounds are toxic and can be teratogenic and carcinogenic to organisms [26–29], so they are regulated by various environmental protection agencies. Current studies have found that liquid and gas chromatography, capillary electrophoresis, and electrochemical methods can be used to detect phenol and its derivatives [30–36]. They have high sensitivity for the detection of phenol, but the detection process is complicated and time-consuming. Therefore, it is very necessary to accurately and quickly detect phenolic organic pollutants such as phenol.

Herein, we designed a polymer resin sphere coated with aniline for pyrolysis to produce spongy Fe/NPCs nanozymes

✉ Zhengbo Chen
czb979216@sina.com

✉ Xia Zuo
zuoxia@cnu.edu.cn

[1] Department of Chemistry, Capital Normal University, Beijing 100048, China

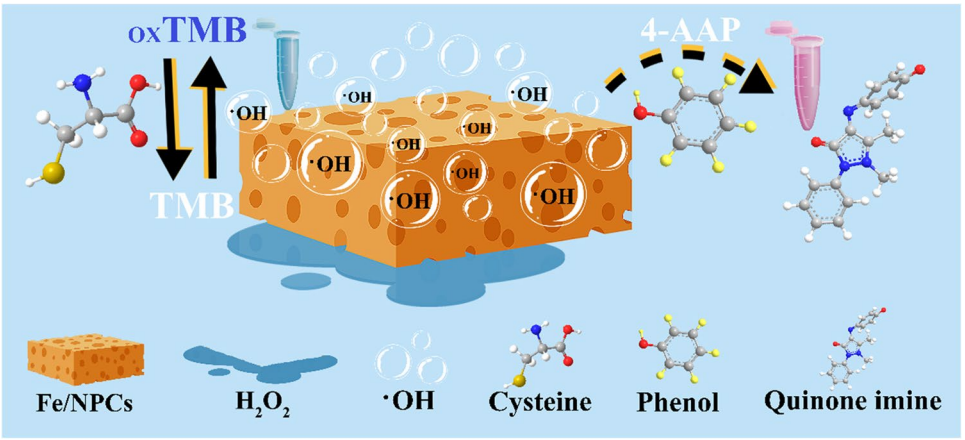

Scheme 1 Schematic diagram of the principle of colorimetric recognition of cysteine and phenol based on sponge-like Fe/NPCs nanozymes sensing

doped with nitrogen and phosphorus double heteroatoms. The nanozymes exhibited good peroxidase activity and oxidase activity due to the synergistic effect of multiple heteroatoms and the coordination of metals. A highly sensitive and specific quantitative assay for cysteine and phenol was developed by the peroxidase-like activity of Fe/NPCs nanozymes. Surprisingly, the nanozymes have achieved accurate determination of phenol and cysteine in tap water and serum, which is of outstanding practical value in both biological and environmental fields.

Experimental section

Materials

Phenol (Phe), 4-aminoantipyrine (4-AAP), ammonium persulfate (APS), 3,3′,5,5′-tetra-methylbenzidine (TMB), acetate, and sodium acetate were obtained from Aladdin. L-Cysteine, o-phenylenediamine (OPD), 2,2′-azinobis (3-ethylbenzothiazoline-6-sulfonic acid ammonium salt (ABTS), aniline, and 4,4′-(hexafluoroisopropylidene) diphenol (BPAF) were purchased from innochem. Hexachlorocyclotriphosphazene (HCCP), triethylamine (TEA), iron chloride hexahydrate ($FeCl_3{\cdot}6H_2O$) were obtained from Alfa. The above reagents are of analytical grade. In addition, the tap water used in the manuscript was collected from the laboratory, and the fetal bovine serum was purchased from Sigma-Aldrich.

Preparation of Fe/NPCs nanozymes

NPCs were prepared according to the method described in our previous report [37]. The prepared NPCs samples were placed in 0.1 M $FeCl_3$ solution and stirred for 12 h to coordinate the metal ions with polyaniline. After that, they were washed several times with 3 M hydrochloric acid and deionized water, and placed in a vacuum oven at 60 °C overnight. The final product was denoted as Fe/NPCs.

Peroxidase-like activity analysis of Fe/NPCs nanozymes

Firstly, TMB (0.5 mM, 50μL) and H_2O_2 (0.05 mM, 100μL) were sequentially added to the HAc-NaAc buffer solution (0.2 M, 750 μL, pH = 4.0). Then, Fe/NPCs (0.5 mg/mL, 50 μL) were injected into the above solution and incubated for 20 min. In contrast, TMB, TMB and H_2O_2, TMB and Fe/NPCs, and Fe/NPCs were analyzed under the same conditions. At the same time, PANI and NPCs were used to replace Fe/NPCs under the same conditions to compare peroxidase-like activity. Using an ultraviolet spectrophotometer, the characteristic absorbance of oxTMB was recorded at 652 nm.

Kinetic analysis of Fe/NPCs nanozymes

By changing the concentrations of TMB and H_2O_2, the kinetics of the peroxidase activity of Fe/NPCs nanozymes was studied. First, Fe/NPCs nanozymes (0.5 mg/mL), TMB as a substrate, a fixed concentration of 0.1 mM H_2O_2, and different concentrations of TMB (0.1, 0.2, 0.3, 0.4, 0.5, 0.6, 0.7, 0.8, 0.9, 1, 2, and 4 mM) were tested and incubated in acetate buffer solution (0.2 M, pH = 4.0) for 5 min. Then, with H_2O_2 as the substrate, Fe/NPCs nanozymes (0.5 mg/mL) were used to immobilize TMB (1 mM), and different concentrations of H_2O_2 (0.005, 0.01, 0.02, 0.03, 0.04, 0.05, 0.06, 0.07, 0.08, 0.09, 0.1, and 0.2 mM) for experimental research. In order to obtain the apparent kinetic parameter, the change of absorbance with time was recorded. Then, the POD activity K_m and V_{max} values of Fe/NPCs nanozymes with TMB and H_2O_2 as substrates were calculated, respectively. The reaction kinetic parameters (K_m and V_{max}) were calculated according to Michaelis–Menten equation (V, V_{max}, $[S]$, and K_m are the initial speed, the maximum reaction speed, substrate

concentration, and the Michaelis constant): $1/V = K_m/V_{max}(1/[S] + 1/K_m)$.

Procedure for the determination of cysteine

In a typical procedure, 50 μL Fe/NPCs nanozymes (0.5 mg/mL), 100 μL H_2O_2 (0.05 mM), and 50 μL TMB (0.5 mM) were added to 750 μL acetic acid buffer solution (0.2 M, pH = 4.0). After the mixed solution was reacted for 3 min at room temperature, 50 μL of cysteine with different concentrations (0, 0.1, 0.5, 1, 1.5, 2, 2.5, 3, 3.5, and 4 μM) was added and incubated for 20 min. The UV–Vis absorption signal at 652 nm was monitored, and each analyte was measured in five replicates. The data were normalized to $A_{0,652\ nm}$–$A_{i,652\ nm}$ to eliminate potential bias caused by differences in the raw absorbance of the blank solution.

Procedure for the determination of phenol

Firstly, 50 μL 0.05 mM H_2O_2 and 200 μL 6 mM 4-AAP were added to 500 μL NaAc-HAc buffer (0.2 M, pH = 4.8), and then, 50 μL of 0.5 mg/mL Fe/NPCs nanozymes was added to mix well. Then, 200 μL of different concentrations of phenol (0.05, 0.5, 2, 4, 6, 8, and 10 μM) was mixed and incubated for 20 min, and then, the UV–Vis absorption solution (λ_{max} = 515 nm) was recorded, and 5 parallel repeated measurements for each analyte to reduce measurement errors were performed. In order to eliminate the absorbance signal caused by the blank sample, the data was standardized during processing, i.e., $A_{i,515\ nm}$–$A_{0,515\ nm}$.

Results and discussion

Synthesis and characterization

Figure 1A shows the SEM image of PZAF particles. The results show that PZAF has a spherical structure with a smooth surface. They are uniform in size and have an average diameter of 2–3 μM. Fig. S1 shows that before carbonization, the surface of PZAF is covered by polyaniline, showing an irregular morphology, but it can be seen that there are still some PZAF particles on the surface. Then, the apparent morphology of the synthesized Fe/NPCs was observed by TEM and SEM. Fig. S2 shows that the nanozyme is an amorphous porous structure, which is wrapped in a thin nano-layer. As shown in Fig. 1B, C, after carbonization and doping of metal Fe, a spherical porous structure was formed on the surface of Fe/NPCs, which effectively increased the specific surface area of the nanozymes. It is more noteworthy that the size of these spherical pores is approximately the same as that of the PZAF particles, which can be attributed to the partial pyrolysis of the PZAF particles during the carbonization process. In addition, in the HRTEM spectrum of the prepared Fe/NPCs nanozymes, N, P, O, C, and Fe elements can be clearly detected (Fig. 1D).

The XRD pattern shows that the sample has two obvious diffraction peaks at $2\theta = 24.4°$ and 43.8° (Fig. 2A), which correspond to the (002) and (100) reflections of the carbon phase, respectively, indicating the formation of graphitic carbon, which further proves the production of amorphous carbon [37]. The diffraction peaks of Fe/NPCs nanozymes are stronger and sharper, indicating

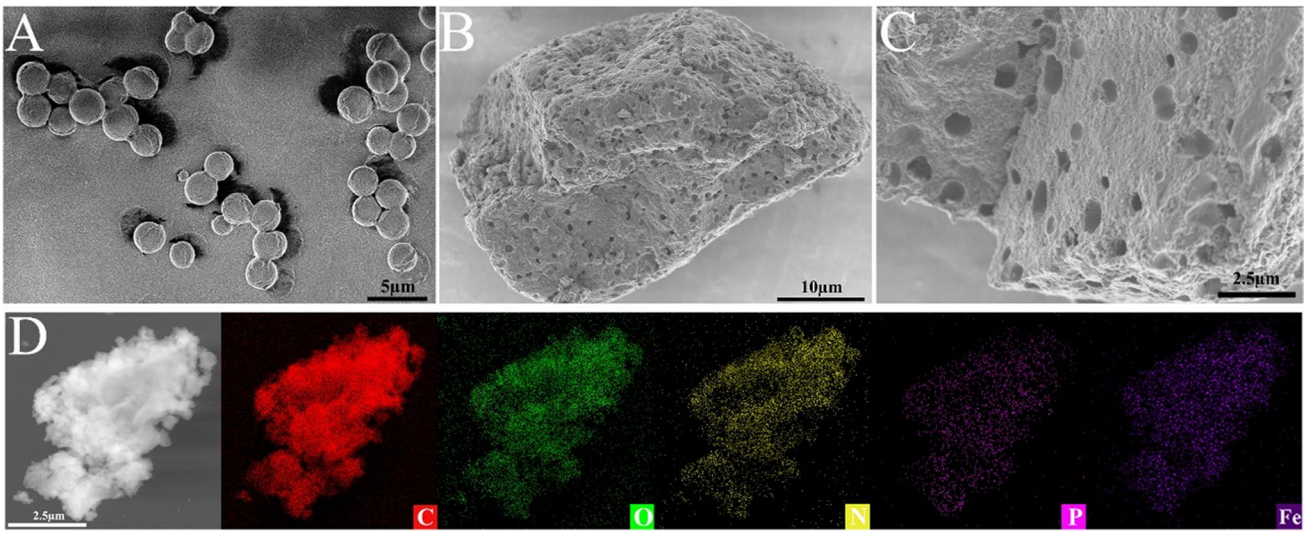

Fig. 1 (A) A typical SEM image of PZAF particles; (B, C) The typical SEM images of Fe/NPCs nanozymes; (D) HRTEM images and corresponding EDS elemental mapping of Fe, N, P, and C atoms

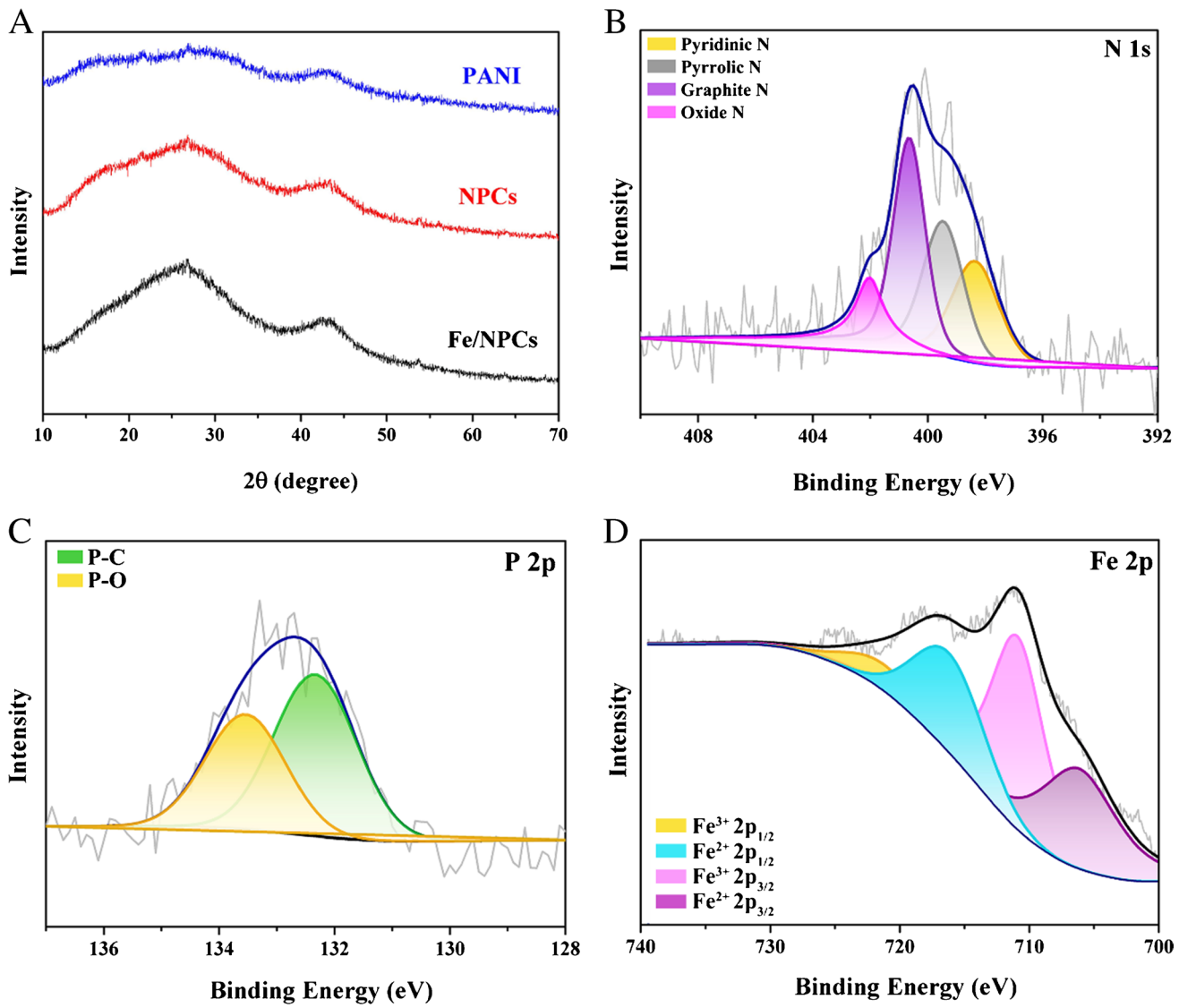

Fig. 2 (A) XRD patterns of PANI, NPCs, and Fe/NPCs. The high-resolution XPS survey spectra in the N 1 s (B), P 2p (C), and Fe 2p (D) of Fe/NPCs nanozymes

that iron doping has an effect on the graphitized structure. Fe increases the soluble carbon content during the high-temperature carbonization process, thereby forming a graphite structure [38]. It is worth noting that other diffraction peaks are not found, indicating that there is no microcrystal of iron-containing species. This can be attributed to the fact that part of the iron species with thin surface was washed away by acid, and part of its iron was doped into the graphite layer during high-temperature pyrolysis, which is consistent with the TEM data.

XPS measures the elemental composition and chemical state of Fe/NPCs nanozymes. The measured spectrum confirmed the presence of C, N, O, P, and Fe in the sample (Fig. S3). In addition, the N 1 s peak of the sample (Fig. 2B) can be fitted to four peaks: pyridine-N (398.35 eV), pyrrole-N (399.47 eV), graphite-N (400.65 eV), and nitrogen oxide (402.03 eV) [39]. Figure 2C shows the XPS spectrum of P 2P. They can be unwound into two forms of P, denoted as PC (132.34 eV) and PO (133.54 eV). This result proves that P was successfully doped into the carbon framework, produce more active centers, and improve the catalytic performance. The high-resolution Fe 2p spectrum of Fe/N/C (Fig. 2D) has characteristic peaks of Fe^{2+} and Fe^{3+}, which can be divided into 721.18 eV (Fe^{3+} $2p_{1/2}$), 716.19 eV (Fe^{2+} $2p_{1/2}$), 710.93 eV (Fe^{3+} $2p_{3/2}$), and 706.16 eV (Fe^{2+} $2p_{3/2}$); Fe–N coordination exists on the surface [40].

Simulated peroxidase activity of Fe/NPCs nanozymes

Fe/NPCs nanozymes can be used as materials to simulate peroxidase activity. As shown in Fig. 3A, the typical TMB is used as a probe for measurement. In the Fe/NPCs nanozymes/TMB/H_2O_2 system, there is an obvious UV–Vis absorption intensity signal at 652 nm. Similarly, weak absorption intensity was obtained without H_2O_2, but no obvious signal was produced in the other control groups. This result proved that Fe/NPCs nanozymes have both excellent peroxidase-like activity and oxidase-like activity. Due to the outstanding peroxidase activity, we subsequently conducted a targeted study on the application of this activity. Figure 3B shows that different chromogenic substrates ABTS and OPD can be catalyzed by Fe/NPCs nanozymes, the color changes from colorless to green or yellow, and the maximum absorption wavelengths are 415 nm and 447 nm, respectively. At the same time, we compared the peroxidase-like activities of PANI and NPCs under the same conditions, which was significantly lower than those of Fe/NPCs nanozymes, indicating that the synergistic effect of heteroatoms N and P and metal interaction improved the performance of peroxidase (Fig. S4).

As we all know, the catalytic mechanism of Fe/NPCs nanozymes as peroxidases may be the oxidation of H_2O_2 to produce active intermediates ·OH. Isopropanol as a typical ·OH trap is used to identify the generation of free radicals. By comparison, it can be seen that the addition of isopropanol results in a significant decrease in the UV–Vis absorption intensity at 652 nm (Fig. S5). These evidences further prove that Fe/NPCs nanozymes can effectively convert H_2O_2 to ·OH. Compared with natural peroxidase, the performance of Fe/NPCs nanozymes also has a high degree of temperature dependence and pH dependence. As shown in Fig. S6, Fe/NPCs nanozymes exhibit the best peroxidase activity at pH = 4.0 and 25 °C. After incubating the reaction system for 20 min, the absorbance tends to a stable value. The above optimized conditions were used as the optimal experimental conditions for the next stage of the experiment.

The apparent steady-state kinetic analysis of Fe/NPCs nanozymes

In order to explore the simulated peroxidase activity of Fe/NPCs nanozymes more deeply, we performed apparent steady-state kinetics of Fe/NPCs nanozymes by changing different concentrations of TMB and H_2O_2 under the same conditions analyzed. After testing, it was found that the rate images with TMB and H_2O_2 as substrates all showed a typical Michaelis–Menten curves (Fig. 4A, C). Afterwards, we process the data and obtain the parameters K_m and V_{max} according to the slope and intercept of the Lineweaver–Burk diagram (Fig. 4B, D). The calculation shows that when TMB and H_2O_2 are used as the base, the maximum enzymatic reaction rate V_{max} of Fe/NPCs nanozymes is 5.6×10^{-8} M·S^{-1} and 9.1×10^{-8} M·S^{-1}, respectively. At the same time, the Michaelis constant K_m obtained with TMB and H_2O_2 as the base is 0.27 mM and 0.033 mM, respectively. The affinity of the enzyme to the substrate can be expressed in K_m. The smaller the K_m value, the stronger the affinity of the enzymes to the substrate. As shown in Table S0, the K_m value of Fe/NPCs nanozymes to TMB is relatively small. Not only that, the K_m value of Fe/NPCs nanozymes for H_2O_2 is more than 100 times

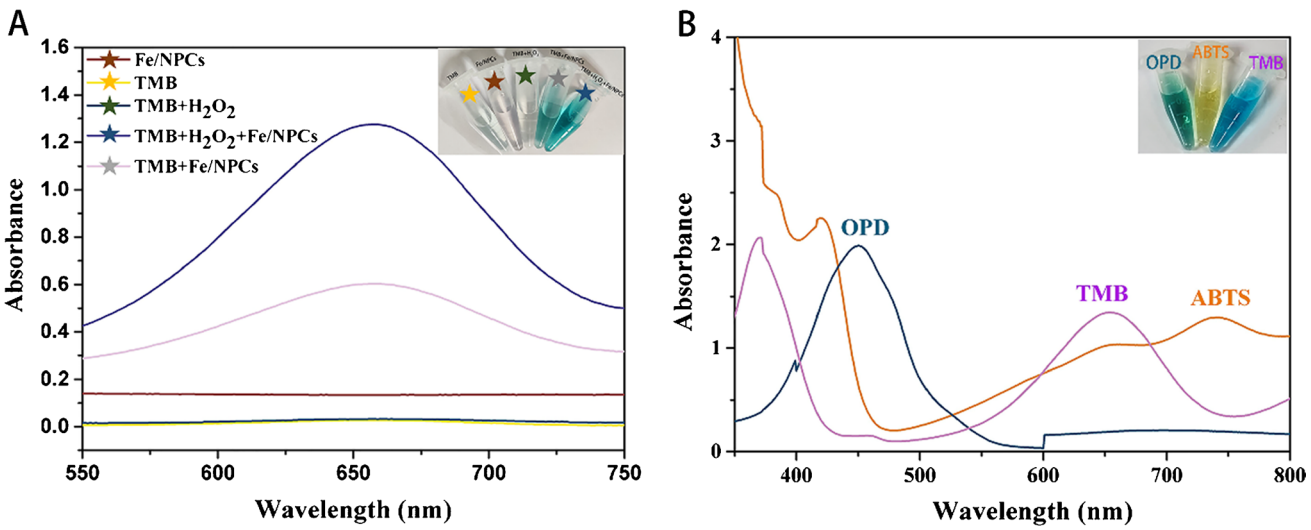

Fig. 3 (A) The UV–visible absorption spectra of Fe/NPCs nanozymes, TMB, TMB + H_2O_2, TMB + Fe/NPCs nanozymes, and TMB + H_2O_2 + Fe/NPCs nanozymes. (B) The UV–Vis absorption spectrum of ABTS, OPD, and TMB catalyzed by Fe/NPCs nanozymes

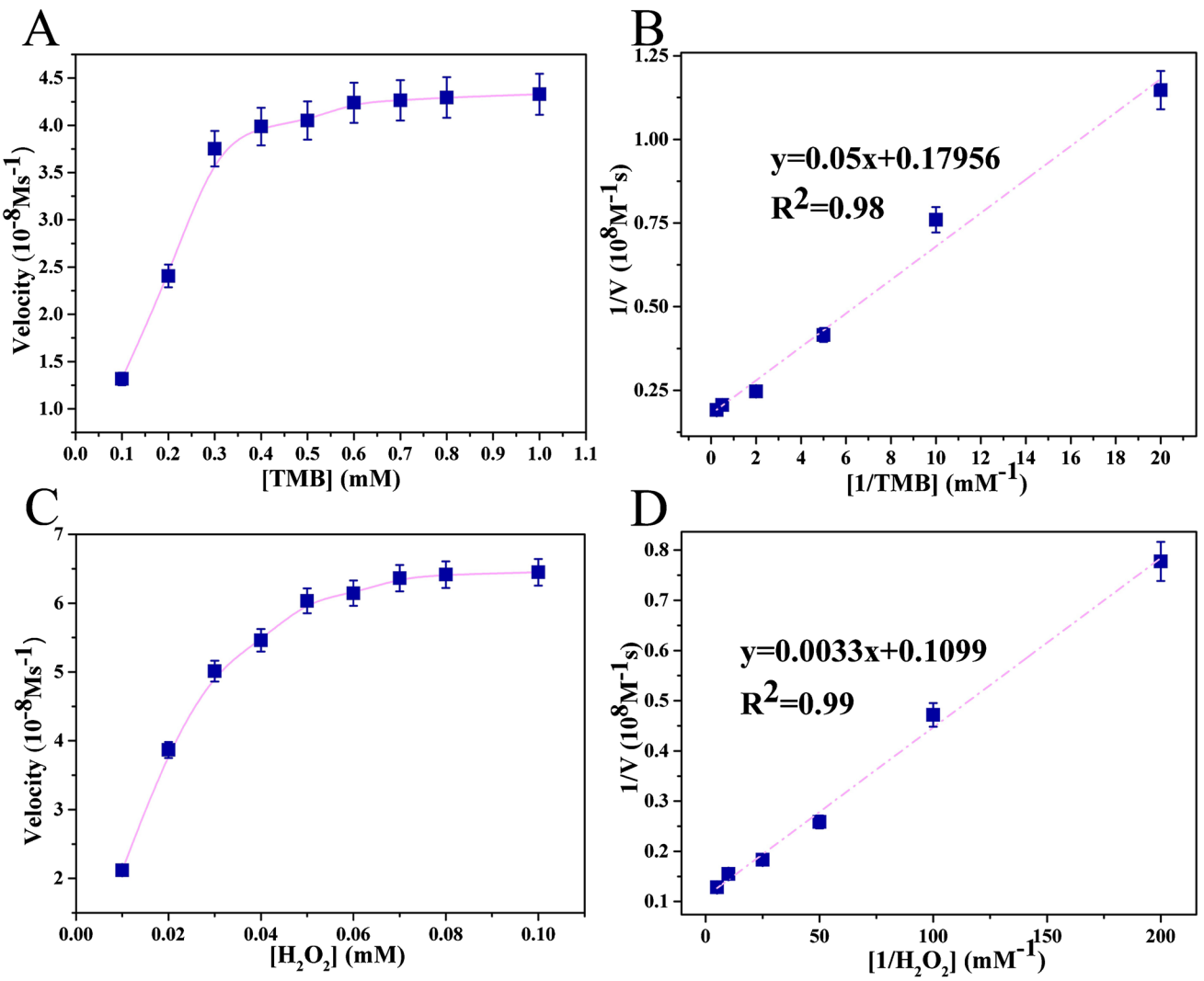

Fig. 4 Lineweaver–Burk graph of Fe/NPCs versus TMB (A) and H_2O_2 (C). Double reciprocal graph of initial reaction rates of TMB (B) and H_2O_2 (D)

lower than that of HRP, and it is also lower than that of other reported materials. This result indicated that Fe/NPCs nanozymes have a better affinity for TMB and H_2O_2, and a more superior mimic peroxidase activity.

Analytical performance of peroxidase activity based on Fe/NPCs nanozymes

Detection of cysteine

Cysteine, as a common amino acid in organisms, contains thiols in its molecular structure and has reducibility, which inhibits the oxidation of TMB and reduces the absorbance response of oxTMB, the principle of detection is shown in Fig. S7. As shown in Table S2 and Fig. 5A, the response ($A_{0,652\ nm}$–$A_{i,652\ nm}$) of the Fe/NPCs nanozyme-based colorimetric sensor to cysteine is positively increased with increasing concentration. In the range of 0.1–4 μM (R^2 = 0.98), the absorbance difference at 652 nm has a linear relationship with cysteine, and the LOD value is 53.6 nM, indicating that the developed colorimetric sensor has a higher sensitivity determination of cysteine (Table S3, Fig. 5B).

To determine the selectivity of the colorimetric sensor, various interfering substances common in the human body including metal ions, glucose, and amino acids were measured (Table S4, Fig. 5C). The experimental results show that the colorimetric detection method based on nanozymes has high selectivity.

Detection of phenol

Fe/NPCs nanozymes have excellent peroxidase activity and good development prospects in the field of environmental detection applications. Based on this property, a colorimetric strategy for quantitative detection of phenol

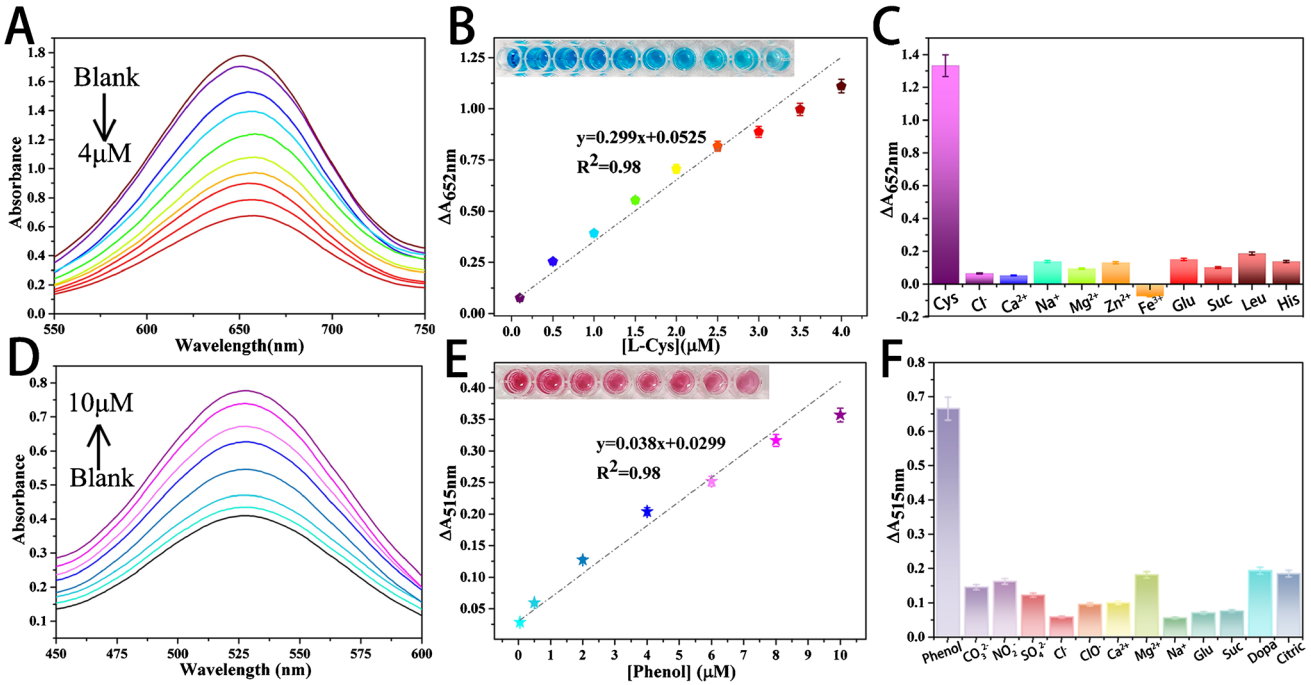

Fig. 5 Fe/NPCs nanozymes are used as peroxidase mimics for the detection of analytes. UV–Vis absorption spectra produced by different concentrations of (A) cysteine and (D) phenol. (B) The linear calibration curve of cysteine in the concentration range of 0.1–4 μM and (E) the linear calibration curve of phenol in the concentration range of 0.05–10 μM. Fe/NPCs nanozymes detect the interference of (C) cysteine and (F) phenol

based on Fe/NPCs nanozymes was designed. Fe/NPCs nanozymes were oxidized and coupled with hydrogen peroxide, phenol, and 4-aminoantipyrine (4-AAP) to form quinone imine, resulting in color change; the principle of detection is shown in Fig. S7. To give full play to the performance of Fe/NPCs nanozymes for phenol detection under optimal conditions, we systematically explored the effects of pH, 4-AAP concentration, H_2O_2 concentration, and other parameters on the activity (Fig. S8). As shown in Fig. 5D, the UV–Vis absorption intensity ($A_{i,515\ nm}$–$A_{0,515\ nm}$) increased with the increase of phenol concentration, and the intensity got higher and higher. Table S5 and Fig. 5E show that in the concentration range of 0.05–10 μM, the UV–Vis absorption intensity has a good linear relationship with the phenol concentration ($R^2 = 0.98$). According to the 3σ rule, the detection limit of the sensor system for phenol was calculated to be 5.4 nM.

In order to test the selectivity of this sensing strategy to phenol, potential interferences such as common anions and cations and biomolecules in tap water were selected. As shown in Table S6 and Fig. 5F, under the best experimental conditions, CO_3^{2-}, NO_2^-, SO_4^{2-}, Cl^-, ClO^-, Ca^{2+}, Mg^{2+}, Na^+, glucose, sucrose, dopamine, and citric acid at a concentration of 100 μM as interference substances were added, and the phenol concentration was 10 μM. Although the absorbance of these interferences had a certain signal, it did not affect the accurate detection of phenol.

As listed in Table S1, the Fe/NPCs nanozymes have a wide detection range at low concentrations of cysteine and phenol and have a lower detection limit than other assays.

Application test in real environment

To evaluate the test performance of the sensor in actual samples, we tested cysteine in serum. First, we filtered the serum sample through a 0.22-mm nitrocellulose membrane to remove physical impurities, and then diluted it 100 times with PBS (pH = 7.4) buffer for use. Four different concentrations of cysteine were spiked into serum samples, and different absorbance response values were generated between 0.5 and 2 μM, and the recoveries were 104.3 to 107.6% (Table 1, Table S4).

Phenol was also detected in the real environment, the tap water was collected from the laboratory, and after simple filtration treatment, the accuracy reached between 89.5 and 96.7% in the low concentration range of 0.05–2 μM (Table 1, Table S7).

Fe/NPCs nanozymes can not only detect cysteine in serum, but also detect phenol in tap water. In addition, the best reference value of cysteine in biomedicine is less than 6.3 μmol L^{-1}. According to national water quality standards,

Table 1 The application of this sensing strategy to determination of phenol and cysteine in tap water and serum

Sample	Measuring substance	Added (μM)	Detected[a±b] (μM)	Recovery (%)
Serum	L-Cysteine	0.5	0.53 ± 0.0033	105.8
		1	1.06 ± 0.0032	106.2
		1.5	1.61 ± 0.0023	107.6
		2	2.09 ± 0.0029	104.3
Tap water	Phenol	0.05	0.045 ± 0.0019	89.5
		0.5	0.48 ± 0.0013	96.3
		1	0.95 ± 0.0019	95
		2	1.93 ± 0.0025	96.7

[a±b]Mean ± standard deviation of five independent measurements

the phenol content in tap water should not exceed 0.002 mg L^{-1}. The detection limit of the sensing strategy is lower than the critical value, and the sensitivity is high, which has excellent development potential in the field of biology and environment.

Conclusion

In summary, we develop a variety of heteroatom-doped and metal-ligated nanozymes, which provide a new idea to improve the activity of carbon nanozymes. Based on this, the colorimetric sensor achieved accurate detection of cysteine and phenol, which is due to the good peroxidase activity of Fe/NPCs nanozymes. In addition, highly sensitive detection of phenol and cysteine was also accomplished in real samples, which has potential applications in biological and environmental fields.

Supplementary Information The online version contains supplementary material available at https://doi.org/10.1007/s00216-022-04074-8.

Funding This work was financially supported by the Natural Science Foundation of Beijing Municipality (no. 2192010 and no. 2182012), the National Natural Science Foundation (no. 11179033), and Capacity Building for Sci-Tech Innovation-Fundamental Scientific Research Funds, Scientific Research Project of Beijing Educational Committee (KM202010028007).

Declarations

The authors declare no competing interests.

References

1. Gao L, Zhuang J, Nie L, Zhang J, Zhang Y, et al. Intrinsic peroxidase-like activity of ferromagnetic nanoparticles. Nat Nanotechnol. 2007;2:577–83.
2. Wang H, Wan K, Shi X. Recent advances in nanozyme research. Adv Mater. 2019;31:1805368.
3. Zhang Z, Zhang X, Liu B, Liu J. Molecular imprinting on inorganic nanozymes for hundred-fold enzyme specificity. J Am Chem Soc. 2017;139:5412–9.
4. Zhang J, Wu S, Lu X, Wu P, Liu J. Manganese as a catalytic mediator for photo-oxidation and breaking the pH limitation of nanozymes. Nano Lett. 2019;19:3214–20.
5. Wu JH, Lv WX, Yang QT, et al. Label-free homogeneous electrochemical detection of microRNA based on target-induced anti-shielding against the catalytic activity of two-dimension nanozyme. Biosens Bioelectron. 2021;171:112707.
6. Zhang H, Liang X, Han L, Li F. "Non-naked" gold with glucose oxidase-like activity: a nanozyme for tandem catalysis. Small. 2018;14:1803256.
7. Lu N, Zhang M, Ding L, Zheng J, Zeng C, et al. Yolk–shell nanostructured Fe_3O_4@C magnetic nanoparticles with enhanced peroxidase-like activity for label-free colorimetric detection of H_2O_2 and glucose. Nanoscale. 2017;9:4508–15.
8. Wu JH, Yang QT, Li Q, Li HY, Li F. Two-dimensional MnO2 nanozyme-mediated homogeneous electrochemical detection of organophosphate pesticides without the interference of H2O2 and color. Anal Chem. 2021;93:4084–91.
9. Hu Y, Gao XJ, Zhu Y, Muhammad F, Tan S, Cao W, et al. Nitrogen-doped carbon nanomaterials as highly active and specific peroxidase mimics. Chem Mater. 2018;30:6431–9.
10. Lin L, Song X, Chen Y, Rong M, Zhao T, et al. Intrinsic peroxidase-like catalytic activity of nitrogen-doped graphene quantum dots and their application in the colorimetric detection of H_2O_2 and glucose. Anal Chim Acta. 2015;869:89–95.
11. Fan K, Xi J, Fan L, Wang P, Zhu C, Tang Y, et al. Vivo guiding nitrogen-doped carbon nanozyme for tumor catalytic therapy. Nat Commun. 2018;9:1440–50.
12. Zhu DQ, Zhang ML, Pu L, Gai PP, Li F. Nitrogen-enriched conjugated polymer enabled metal-free carbon nanozymes with efficient oxidase-like activity. Small. 2021;18:2104993.
13. Li W, Wang D, Zhang Y, Tao L, Wang T, et al. Defect engineering for fuel-cell electrocatalysts. Adv Mater. 2020;32:1907879.
14. Liu Z, Ai J, Sun M, Han F, Li Z, Peng Q, et al. Phosphorous-doped graphite layers with outstanding electrocatalytic activities for the oxygen and hydrogen evolution reactions in water electrolysis. Adv Funct Mater. 2020;30:1910741.
15 Liu XF, Antonietti M. Molten salt activation for synthesis of porous carbon nanostructures and carbon sheets. Carbon. 2014;69:460–6.
16. Qu K, Zheng Y, Zhang X, Davey K, Dai S, Qiao SZ. Promotion of electrocatalytic hydrogen evolution reaction on nitrogen-doped carbon nanosheets with secondary heteroatoms. ACS Nano. 2017;11:7293–300.
17. Gao K, Wang B, Tao L, Cunning BV, Zhang Z, et al. Efficient metal-free electrocatalysts from N-doped carbon nanomaterials: mono-doping and co-doping. Adv Mater. 2019;31:1805121.
18. Zhang CH, Liu WD, Chen CX, Ni PJ, et al. Emerging interstitial/substitutional modification of Pd-based nanomaterials

with nonmetallic elements for electrocatalytic applications. Nanoscale. 2022;14:2915–42.
19. Zhang XH, Li QG, Hou DY. Effects of feed solution pH and draw solution concentration on the performance of phenolic compounds removal in forward osmosis process. J Environ Chem Eng. 2017;5:2508–14.
20. Zhang CS, Wang XJ, Wang LG. Removal of phenolic substances from wastewater by algae. Environ Chem Lett. 2020;18:377–92.
21. Lu Y, Yan LH, Zhang JF. Biodegradation of phenolic compounds from coking wastewater by immobilized white rot fungus Phanerochaete chrysosporium. J Hazard Mater. 2009;165:1091–7.
22. Tian HL, Xu XJ, Li BA. Biodegradation of phenolic compounds in high saline wastewater by biofilms adhering on aerated membranes. J Hazard Mater. 2020;392:122463.
23. Rahmanian N, Jafari SM, Galanakis CM. Recovery and removal of phenolic compounds from olive mill wastewater. J Am Oil Chem Soc. 2014;91:1–18.
24. Ma XY, Zhang XW, Ye L, et al. Phenolic compounds promote the horizontal transfer of antibiotic resistance genes in activated sludge. Sci Total Environ. 2021;800:149549.
25. Liu S, Huang BY, Liang L, et al. Nanocapsulation of horseradish peroxidase (HRP) enhances enzymatic performance in removing phenolic compounds. Int J Biol Macromol. 2020;150:814–22.
26. Alshabib M, Onaizi SA. A review on phenolic wastewater remediation using homogeneous and heterogeneous enzymatic processes: current status and potential challenges. Sep Purif Technol. 2019;219:186–207.
27. Salehi S, Abdollahi K, Mokhtarani B, et al. Applications of biocatalysts for sustainable oxidation of phenolic pollutants: a review. Sustainability. 2021;13:8620.
28. Paisio CE, Agostini E, Bertuzzi ML, et al. Lethal and teratogenic effects of phenol on Bufo arenarum embryos. J Hazard Mater. 2009;167:64–8.
29. Nesvera J, Rucka L, Patek M. Catabolism of phenol and its derivatives in bacteria: genes, their regulation, and use in the biodegradation of toxic pollutants. Adv Appl Microbiol. 2015;93:107–60.
30. Paterson B, Cowie CE, Jackson PE. Determination of phenols in environmental waters using liquid chromatography with electrochemical detection. J Chromatogr A. 1996;731:95–102.
31. Fukushi K, Yakushiji Y, Saito K, et al. Simultaneous determination of a pyridine-triphenylborane anti-fouling agent and its estimated degradation products using capillary zone electrophoresis. J Chromatogr A. 2010;1217:2187–90.
32. Chen K, Zhang ZL, Liu W, et al. A graphene-based electrochemical sensor for rapid determination of phenols in water. Sensors. 2013;13:6204–16.
33. Xiao X, Wang YH, Tong ZW, et al. Synthesis of pumpkin-like CeO2 microstructures and electrochemical detection for phenol. Inorg Nano-Met Chem. 2019;49:349–53.
34 Seebunrueng K, Dejchaiwatana CH, Santaladchaiyakitb Y, Srijaranai S. Development of supramolecular solvent based microextraction prior to high performance liquid chromatography for simultaneous determination of phenols in environmental water. RSC Adv. 2017;7:50143–9.
35. Cesarino I, Moraes FC, Machado SAS, et al. Real-time electrochemical determination of phenolic compounds after benzene oxidation. J Electroanal Chem. 2012;672:34–9.
36. Zhang Y, Yang KL. Quantitative detection of phenol in wastewater using square wavevoltammetry with pre-concentration. Anal Chim Acta. 2021;1178:338788.
37. Ma J, Yu Y, Chen CL, Zuo X, et al. Using multifunctional polymeric soft template for synthesizing nitrogen and phosphorus co–doped mesoporous carbon frameworks electrocatalysts for oxygen reduction reaction. ChemistrySelect. 2018;3:9013–20.
38. Suk Jung W, Popov BN. Improved durability of Pt catalyst supported on N-doped mesoporous graphitized carbon for oxygen reduction reaction in polymer electrolyte membrane fuel cells. Carbon. 2017;122:746–55.
39. Deng C, Zhong H, Li X, Yao L, Zhang H. A highly efficient electrocatalyst for oxygen reduction reaction: phosphorus and nitrogen co-doped hierarchically ordered porous carbon derived from an iron-functionalized polymer. Nanoscale. 2016;8:1580–7.
40. Zhang H, Wang T, Wang J, Liu H, Dao TD, et al. Surface-plasmon-enhanced photodriven CO_2 reduction catalyzed by metal–organic-framework-derived iron nanoparticles encapsulated by ultrathin carbon layers. Adv Mater. 2016;28:3703–10.